

A high energy density 3D nano-carbon based magnesium hydroxide reversible chemical reaction heat storage material synthesis and heat transfer performance investigation

Shijie Li ^a, Xiangyu Yang ^{a,b}, Xinyu Li ^a, Wenshan Qu ^a, Tao Zhou ^a, Ti Dong ^c, Lisheng Deng ^d, Jin Zhang ^{a,*}, Jianguo Zhao ^{a,b,*}

^a Institute of Carbon Materials Science, Shanxi Datong University, Datong 037009, China

^b School of Materials Science and Engineering, Taiyuan University of Technology, Taiyuan 030024, China

^c Key Laboratory of Renewable Energy, Guangdong Provincial Key Laboratory of New and Renewable Energy Research and Development, Guangzhou Institute of Energy Conversion, Chinese Academy of Sciences, No. 2 Nengyuan Rd., Wushan, Tianhe District, Guangzhou 510640, China

^d Guangdong Intelligent Filling Technology Limited Company, No. 63 (F3) 5, Zone C, Sanshui Industrial Park, Foshan, Guangdong 528137, China



ARTICLE INFO

Keywords:

3D-carbon nano-materials

Heat transfer numerical simulation

Thermal energy storage, magnesium hydroxide

ABSTRACT

Magnesium hydroxide composite chemical heat storage materials were constructed with in-situ prepared 3D-Graphene. Mg(OH)₂ particles were anchored onto the surface of the nanosupport by deposition-precipitation method. According to the heat transfer numerical simulation, addition of 3D-Graphene could greatly change the temperature distribution in the reactor and was easier to export thermal energy to the outside thermal load side. This energy storage system could output thermal energy at around 200 °C and absorbed heat at the range of 300–400 °C. Transmission electron microscopy result indicated that the particle size of Mg(OH)₂ was primarily in the range of 20–50 nm. X-ray diffraction characterization showed that the magnesium hydroxide was well dispersed in the composite material. This material provided an obviously enhanced heat storage density (610 kJ/kg), no distinct attenuation and greatly improved hydration rate compared with those of magnesium oxide because of hydrogen bonding effect in composite materials. 3D-Graphene lead to obvious decomposition activation energy decreasing of Mg(OH)₂ that would improve its utilization in the heat storage process. This was probably due to its surface effect. 3D-Graphene/Mg(OH)₂-1 showed the lowest activation energy (116.7 kJ/mol). The thermal conductivity of the composite material was 9.4 times higher than that of Mg(OH)₂ as a result of the addition of 3D-Graphene. The proposed method provided a facile and valid technique for thermal energy utilization and the synthesis of nano-composed materials with enhanced chemical heat storage performance.

1. Introduction

The development of solar energy and other renewable energy utilization technology have become more important with the increasing consumption of conventional energy resources and also a great scientific challenge for our period [1,2]. As an important aspect of this field, thermal energy storage has attracted considerable attention. It consists mainly of three types: sensible heat storage [3,4], latent heat storage [5,6], and chemical heat storage [7,8]. When contrasting chemical heat storage with the other two energy storage technologies, chemical heat storage shows high energy efficiency and a high level of heat storage density [9]. Because materials are an important part of thermal energy

storage technologies, many have been researched [10–14].

Balasubramanian et al [15] using low hydrated MgSO₄ as the heat storage model, the heat and mass transfer and hydrolysis kinetics in the chemical heat storage process were solved by finite difference method. The results showed that the heat diffusion was the dominant factor in the whole reaction heat transfer process, and the reaction was also affected by the desorption kinetics. Farcot and other researchers [16] studied the heat and mass transfer mechanism of hydrophilic inorganic salt SrCl₂·H₂O in an open continuous cross flow moving bed reactor. Two-dimensional modeling of the reactor was carried out by using the finite element method. Their research supported that the inlet pressure of the reactor and the partial pressure of steam had a great influence on

* Corresponding authors at: Institute of Carbon Materials Science, Shanxi Datong University, Datong 037009, China.

E-mail addresses: zhangjing8014484@163.com (J. Zhang), zhaojianguo@sxtdx.edu.cn (J. Zhao).

thermal storage reaction behavior. The mass transfer process was the main factor controlling the performance of open reactor. Malley erwien et al [17]. studied the influence of heat and mass transfer factors such as pressure loss and temperature distribution on the design of the reactor in the process of chemical heat storage of hydrophilic inorganic salts. All results of the study indicated that the increase of the number of reaction beds and the increase of bed compactness were conducive to the improvement of thermal energy storage reactor performance. Lehmann et al [18]. proposed an axisymmetric model of mass and heat transfer in a packed bed of composite adsorbent particles for the study of crystalline hydrated salt porous material composite thermal storage material ($\text{CaCl}_2/\text{Ca-X}$ molecular sieve), and gave the adsorption equilibrium and kinetic model of this composite material. This model can be used to predict the heat storage and release behavior of hydrophilic salt porous composites. Kubota et al. added some porous carbon and hydrophilic material in LiOH for low temperature thermal energy utilization and these materials showed greatly improved heat storage performance [19, 20]. These results showed that the additive could improve the overall heat and mass transfer and reaction performance of the materials. And the choice of energy storage materials and additives is particularly important. Magnesium hydroxide, as a high-temperature heat storage material, presents both low reaction rate and thermal conductivity during the reaction [21,22], hence, the synthesis of modified $\text{Mg}(\text{OH})_2$ based materials with high heat storage density and enhanced heat transfer performance has great value. The system design with rapid heat release ability at high temperature for efficient thermal energy conversion and storage remains a challenge.

3D-carbon nanotube sponges, arrays, as well as graphene [23–25], as typical three-dimensional nanomaterials with stable physical and chemical properties [26–29], were used in many fields, including electronics [30–32] and catalysis [28,33,34]. However, 3D carbon nanomaterials were seldom applied for heat storage [35,36], especially for high-temperature thermochemical heat storage. In this work, $\text{Mg}(\text{OH})_2$ and its derived chemical heat storage materials have been considered and investigated. The energy storage mechanism was based on dehydration/hydration reversible chemical reaction of $\text{Mg}(\text{OH})_2$. This process accompanied with heat absorption and heat releasing, which was expressed as following chemical reaction equation. In this reaction equation, ΔH stood for enthalpy change of the chemical reaction.



During the material preparing process a 3D carbon nanomaterial (3D-Graphene) and $\text{Mg}(\text{OH})_2$ were selected, 3D-Graphene/ $\text{Mg}(\text{OH})_2$ composite nanomaterial was synthesized. And the performance and structure of the material were tested. Further, heat transfer numerical simulation of 3D-Graphene/ $\text{Mg}(\text{OH})_2$ composite nanomaterial in reactor was carried out.

2. Materials and methods

2.1. Preparation and test of 3D-Graphene/ $\text{Mg}(\text{OH})_2$ composite nanomaterial

Firstly 6 g natural graphite was added in mixture of H_2SO_4 (Sinopharm chemical reagent, Ltd, purity, 98.0%), $\text{K}_2\text{S}_2\text{O}_8$ (Aladdin, Ltd, purity, 99.0%) and P_2O_5 (Aladdin, Ltd, purity, 98.0%) (1.1 mmol:0.02 mmol:0.04 mmol). This mixture was moved into blast furnace at 90 °C for 6 h. This solid was washed with deionized water and filtered, dried at 90 °C then composed with another concentrated sulfuric acid (4.5 mmol). At this time KMnO_4 (Damao chemical reagent factory, purity, 98.0%) (0.19 mmol) was mixed with this composite under stirring at zero degree centigrade. This mixture was heated to 30 °C and kept for 2 h. 125 mL ultrapure water was added in under strong stirring for further 2 h. After that, 400 mL ultrapure water and 80 mL H_2O_2 (Sinopharm chemical reagent, Ltd, purity, 30%) was added. The obtained oxide was purged with hydrochloric acid (Sinopharm chemical reagent, Ltd, 10%,

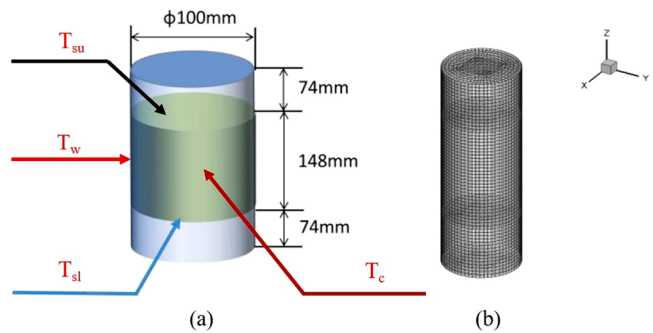


Fig. 1. (a) The physical model and (b) Heat transfer 3D numerical grid of the reactor with heat storage materials.

5 L). Dialysis bag was used to purify the mixture until pH value reached neutral. Finally, GO solution (4 mg/mL) was obtained in the dialysis bag. The GO solution was concentrated to 8 mg/mL and heated to 170 °C for 12 h in a 50 mL hydrothermal reactor. When the reactor cooled to room temperature, refrigerant dryer was used to dry the product and 3D-Graphene was collected.

The next step 3D-Graphene was composed with $\text{Mg}(\text{OH})_2$ by deposition-precipitation method. Magnesium acetate hydrate (400 mg; Aladdin, Ltd., purity, 98.0%) and 3D-Graphene (120 mg) were dissolved in 10 mL DI water. Then, 1800 mg of ammonium hydroxide (Damao chemical reagent factory, purity, 20 wt%) was added slowly under vigorous stirring at 25 °C. After 30 min of stirring, the mixture was centrifuged, washed, and dried in an oven at 200 °C. Finally, the composite 3D-Graphene/ $\text{Mg}(\text{OH})_2$ was obtained ($\text{Mg}(\text{OH})_2$; 47 wt%). Magnesium hydroxide and 3D-Graphene/ $\text{Mg}(\text{OH})_2$ were used as raw materials. Then, MgO and Graphene- MgO were prepared by a temperature-programmed reaction by the decomposition of magnesium hydroxide and 3D-Graphene/ $\text{Mg}(\text{OH})_2$ in a tubular stainless-steel reactor with N_2 gas at 450 °C for 4 h. The dehydrated materials were cooled to 110 °C in an N_2 atmosphere, and water vapor carried with N_2 flow was introduced into the reactor for 20 min as the hydration operation at 0.35 Mpa, 150 °C. After hydration operation, endothermic heat and temperature of the samples were measured by thermogravimetric and differential scanning calorimeter analyzer (TG-DSC; STA-200, Nanjingdazhan co., Ltd.). Surface topography was measured by field-emission scanning electron microscopy (SEM, S-4800, Hitachi Limited). Transmission electron microscopy (TEM) results were obtained with FEI Tecnai G212 instrument operated at 100 kV and JEOL JEM-2100F instrument operated at 200 kV. X-ray diffraction (XRD) analysis was performed on D8 Advance X-ray diffractometer (German Bruker) with Cu target (40 kV, 40 mA). Thermal conductivity was measured by heat flux method (DRL-II, Xiangtan Xiangyi Instrument Co., Ltd.). The activation energy of decomposition reaction was calculated by Ozawa method [37] using Arrhenius's equation.

$$\ln\left(\frac{\beta}{T^2}\right) = \ln\frac{R}{E} \frac{A}{f(a)} - \frac{E}{R} \frac{1}{T} \quad (1)$$

In Eq. (1), E, β , T, R, A, α , $f(\alpha)$, are the activation energy (kJ/mol), heating rate (K/s), temperature (K), ideal gas constant (J/(mol·K)), pre-exponential factor, dehydration conversion and function of dehydration conversion, respectively. During calculation of activation energy, the heating rate was 4 K/min, 6 K/min 8 K/min and 10 K/min, and the activation energy was calculated from the slope ($-E/R$) of this equation. The tested samples were named as $\text{Mg}(\text{OH})_2$, 3D-Graphene/ $\text{Mg}(\text{OH})_2$ -1 (composed heat storage material before hydration/dehydration cycles), 3D-Graphene/ $\text{Mg}(\text{OH})_2$ -2 (composed heat storage material after 20 hydration/dehydration cycles), respectively.

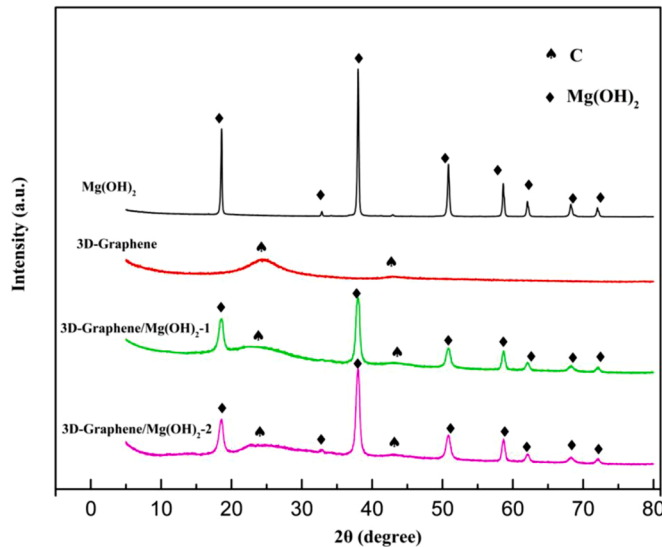


Fig. 2. XRD profiles of Mg(OH)₂, 3D-Graphene, 3D-Graphene/Mg(OH)₂-1 before hydration/dehydration cycles and 3D-Graphene/Mg(OH)₂-2 after 20 cycles hydration/dehydration reaction.

2.2. Heat transfer numerical simulation of 3D-Graphene/Mg(OH)₂ composite nanomaterial in reactor

A stainless-steel cylindrical reactor with internal diameter of 100 mm, height of 300 mm and wall thickness of 2 mm was structured as physical model (Fig. 1a). As shown in Fig. 1a, T_c , T_w stood for core temperature and side inner wall temperature of the reactor filled with heat storage material, respectively. T_{sl} and T_{su} were the lower surface and upper surface temperature of the heat storage material in reactor, respectively. After building of physical model, according to hydration reaction in reactor the heat transfer behavior was simulated. A cylindrical reaction region with nitrogen and reactants as a whole system was established (Fig. 1b). Governing equations of air domain is Eq. (2). The governing equation for the sample region is Eq. (3).

$$\rho_{air}c_{p-air}\frac{\partial T}{\partial t} = \frac{1}{r}\frac{\partial}{\partial r}\left(k_{air}r\frac{\partial T}{\partial r}\right) + \frac{1}{r^2}\frac{\partial}{\partial \varphi}\left(k_{air}\frac{\partial T}{\partial \varphi}\right) + \frac{\partial}{\partial z}\left(k_{air}\frac{\partial T}{\partial z}\right) \quad (2)$$

Where ρ is the air density, kg·m⁻³; C_p is the specific heat capacity, J·kg⁻¹·K⁻¹; T is the temperature, K; t is the time, s; k is the thermal conductivity coefficients, W·m⁻¹·K⁻¹;

$$\begin{aligned} \rho_{sample}c_{p-sample}\frac{\partial T}{\partial t} &= \frac{1}{r}\frac{\partial}{\partial r}\left(k_{sample}r\frac{\partial T}{\partial r}\right) + \frac{1}{r^2}\frac{\partial}{\partial \varphi}\left(k_{sample}\frac{\partial T}{\partial \varphi}\right) + \\ &\quad \frac{\partial}{\partial z}\left(k_{air}\frac{\partial T}{\partial z}\right) + Q_1 + Q_2 \end{aligned} \quad (3)$$

Q_1 is the chemical reaction heat of the sample, Wm⁻³, Q_2 is the built-in heating source of the reactor, Wm⁻³. The composite boundary conditions of the whole heat transfer region are as follows:

$$-k_{air}\left(\frac{\partial T}{\partial r}\right)_{r=R} = h(T - T_f) \text{ and } k_{air}\left(\frac{\partial T}{\partial r}\right)_{r=-R} = h(T - T_f) \quad (4)$$

$$-k_{sample}\left(\frac{\partial T}{\partial r}\right)_{r=R} = h(T - T_f) \text{ and } k_{sample}\left(\frac{\partial T}{\partial r}\right)_{r=-R} = h(T - T_f) \quad (5)$$

$$-k_{shell}\left(\frac{\partial T}{\partial r}\right)_{r=R} = \varepsilon\sigma(T^4 - T_f^4) \quad (6)$$

The initial condition of calculation is as follows:

$$T(r, t) = T_0 \text{ att} = 0 \quad (7)$$

The governing equations of battery three-dimension thermal model

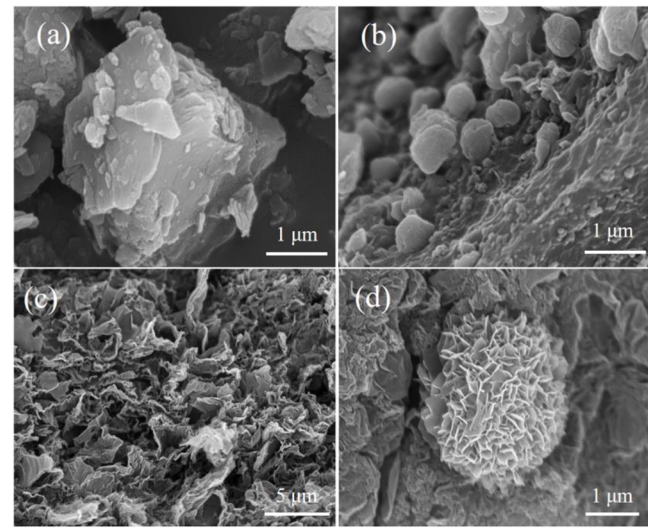


Fig. 3. SEM images of (a) Mg(OH)₂, (b) 3D-Graphene/Mg(OH)₂-1 before hydration/dehydration cycles, (c) 3D-Graphene, (d) 3D-Graphene/Mg(OH)₂-2 after 20 cycles hydration/dehydration reaction, respectively.

were solved in the commercial computational fluid dynamics (CFD) flow solver, Fluent, which was based on the finite volume approximation. In order to speed up the convergence, the 1st order upwind differencing scheme instead of the 2nd order upwind differencing scheme was used to discretize the spatial-derivative term and the calculation error of them is only 0.8 K. Meanwhile, a fully implicit scheme was employed to discretize the transient term. The heat sources were customized by using the user-defined functions (UDFs) available in FLUENT. The numerical elements of samples and air regions were hexahedral. The numerical elements have volume about 1.10×10^{-8} m³ to 1.16×10^{-8} m³ and the total number of numerical meshes is 39,552. Grid-independence tests were conducted to guarantee the employed mesh giving calculation results of adequate accuracy.

3. Results and discussion

3.1. Characterization of 3D-Graphene/Mg(OH)₂ composite nanomaterial

Fig. 2 showed XRD profiles of Mg(OH)₂, 3D-Graphene/Mg(OH)₂, and 3D-Graphene samples. The diffraction peaks at around 18.5°, 32.8°, 38.1°, 50.8°, 58.7°, 62.1°, 68.2°, and 72.2°, respectively, were assigned to Mg(OH)₂ (JCPDS 83-0114). The diffraction peaks at around 25.6° and 43.2° could be attributed to graphitic carbon [38]. It was observed that the diffraction peaks of Mg(OH)₂ became weaker and broader when 3D-Graphene was introduced in. It indicated that Mg(OH)₂ was well dispersed on the 3D-Graphene. After reaction the structure of 3D-Graphene/Mg(OH)₂-2 had no obvious change indicated that this composite material was extremely stable.

Fig. 3a and Fig. 3c showed SEM images of Mg(OH)₂ and 3D-Graphene. The original Mg(OH)₂ existed in big bulk type and 3D-Graphene exhibited three-dimensional porous wrinkle structure. The active components Mg(OH)₂ attached to the graphene surface as nanosheets type (Fig. 3b), and the particle size was much smaller than that of Mg(OH)₂ (Fig. 3a). It could be observed on the surface of 3D-Graphene, Mg(OH)₂ did not damage the structure of 3D-Graphene, but after 20 hydration/dehydration cycles (Fig. 3d) the shape of Mg(OH)₂ particles changed from nanosheets to flower type Fig. 4.(a) showed the TEM image of 3D-Graphene, which existed in flawless Folded lamellar shape. And after loading of Mg(OH)₂ (Fig. 4b-4c) the surface of 3D-Graphene became rough and grainy. Mg(OH)₂ nanoparticles with a main diameter of 20–50 nm were pointed out with red circle in Fig. 4b and Fig. 4c. And some of Mg(OH)₂ particles stacked to bigger sheet into microscale, due

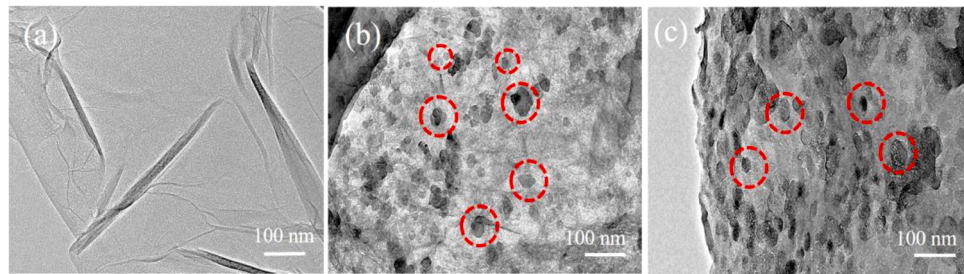


Fig. 4. TEM images of (a) 3D-Graphene, (b) 3D-Graphene/Mg(OH)₂-1 before hydration/dehydration cycles, (c) 3D-Graphene/Mg(OH)₂-2 after 20 cycles hydration/dehydration reaction, respectively.

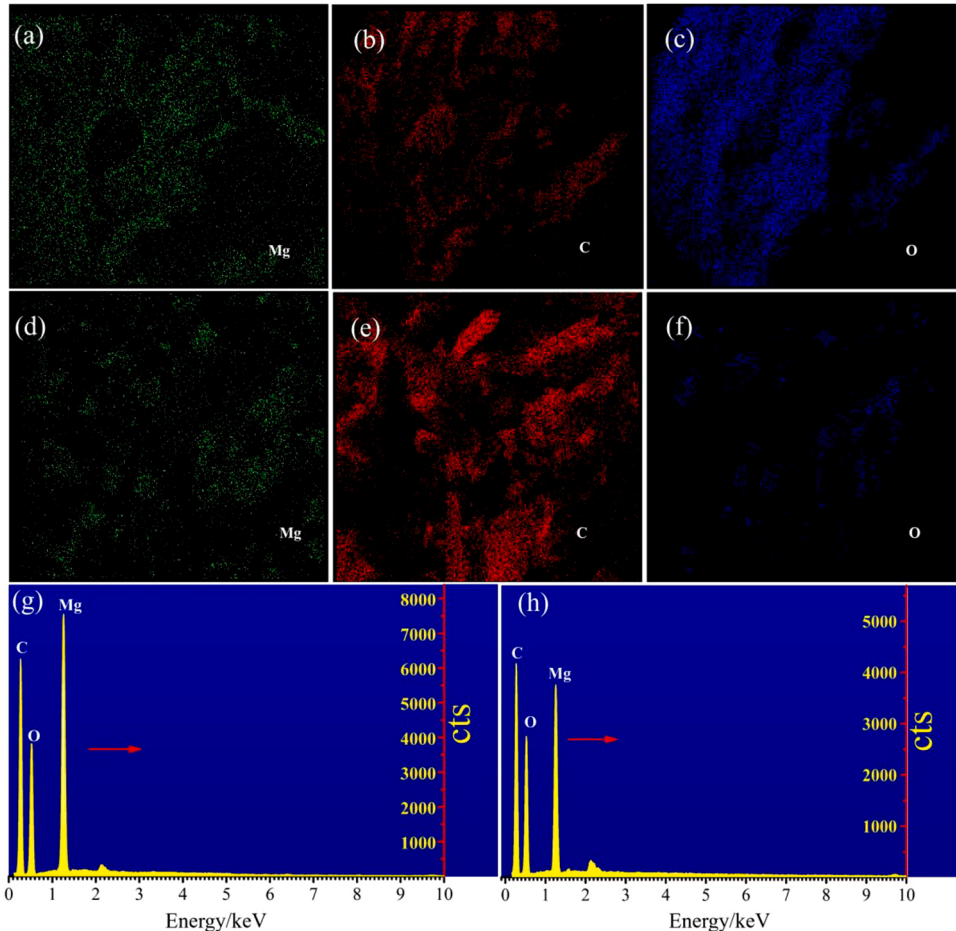


Fig. 5. Element mapping of 3D-Graphene/Mg(OH)₂-1 (a)-(f) before hydration/dehydration cycles, (d)-(f) for 3D-Graphene/Mg(OH)₂-2 after 20 cycles hydration/dehydration reaction; EDS spectrum of (g) 3D-Graphene/Mg(OH)₂-1 and (h) 3D-Graphene/Mg(OH)₂-2.

to the growth and agglomeration of nanoparticles [39] (Fig. 3b). Because of the hydrophilic groups such as hydroxyl, carbonyl, and carboxyl groups on the surface of 3D-Graphene, hydrogen bonding effect [40] could exist between 3D-Graphene and Mg(OH)₂, which strenuously retarded the aggregation of a substantial part of Mg(OH)₂. Thus, great majority of Mg(OH)₂ particles still existed in a nanometer criterion (Fig. 4b-4c) during the composition of 3D-Graphene/Mg(OH)₂.

Fig. 5a-5f were the elements mapping of 3D-Graphene/Mg(OH)₂-1 before hydration/dehydration cycles and 3D-Graphene/Mg(OH)₂-2 after 20 cycles hydration/dehydration reaction, respectively. The principal three elements (Mg, C and O) were existed in the sample, except for Mg from Mg(OH)₂ particles, the element C attributed to 3D-Graphene. And the element O could belong to both Mg(OH)₂ and 3D-Graphene. It could be seen that these three elements in the sample well dispersed

in the form of small grain, even though, when 3D-Graphene/Mg(OH)₂ reacted after 20 hydration/dehydration cycles Fig. 5.g-5h were the EDS spectrum of 3D-Graphene/Mg(OH)₂-1 and 3D-Graphene/Mg(OH)₂-2. X-axis stood for the energy of X-ray and Y-axis was the counts of X-ray photon. EDS analysis (Fig. 5g-5h) showed that the content of C and O on the surface of the sample was higher than Mg. Elements mass ratio for 3D-Graphene/Mg(OH)₂-1 and 3D-Graphene/Mg(OH)₂-2 were $m_C/m_O/m_{Mg}=51.94/36.02/12.05$ and $m_C/m_O/m_{Mg}=49.40/38.58/12.02$, respectively. It proved that the material composition of 3D-Graphene/Mg(OH)₂ had no obvious change and stable after 20 cycles hydration/dehydration reaction.

The surface texture of 3D-Graphene/Mg(OH)₂ were tested by N₂ adsorption/desorption Fig. 6. showed the isotherm of (a) Mg(OH)₂, (b) 3D-Graphene (c) 3D-Graphene/Mg(OH)₂-1 before hydration/

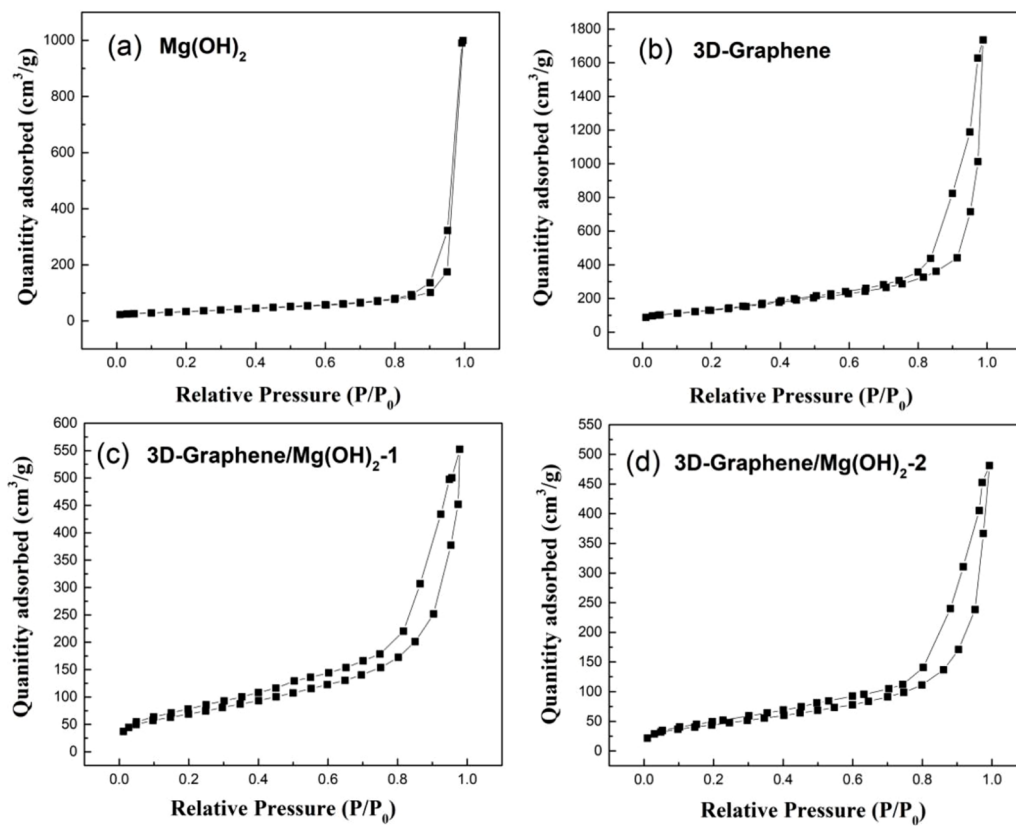


Fig. 6. Nitrogen adsorption desorption of (a) $\text{Mg}(\text{OH})_2$, (b) 3D-Graphene, (c) 3D-Graphene/ $\text{Mg}(\text{OH})_2$ -1 before hydration/dehydration cycles and (d) 3D-Graphene/ $\text{Mg}(\text{OH})_2$ -2 after 20 cycles hydration/dehydration reaction.

Table 1

Surface texture parameters of $\text{Mg}(\text{OH})_2$, 3D-Graphene, 3D-Graphene/ $\text{Mg}(\text{OH})_2$ -1 and 3D-Graphene/ $\text{Mg}(\text{OH})_2$ -2.

Samples	Surface Area (m²/g)	Pore Volume (mL/g)	Average Pore Size (nm)
$\text{Mg}(\text{OH})_2$	42	0.10	0.46
3D-Graphene	235	0.39	15.95
3D-Graphene/ $\text{Mg}(\text{OH})_2$ -1	154	0.23	6.67
3D-Graphene/ $\text{Mg}(\text{OH})_2$ -2	115	0.19	5.31

dehydration cycles and (d) 3D-Graphene/ $\text{Mg}(\text{OH})_2$ -2 after 20 hydration/dehydration cycles. It can be seen that all samples distinguished type II isotherm with hysteresis type H3, hinted slit-shaped mesoporous pore structure. After 20 hydration/dehydration cycles (Fig. 6d), pore structure showed no remarkable destruction or variety. Surface area, pore volume, and average pore size of all samples were showed in Table 1. The synthesis strategy of this composed material really made good use of the high specific surface area of 3D-Graphene ($235 \text{ m}^2/\text{g}$) and pore structure to improve the surface texture of $\text{Mg}(\text{OH})_2$. After modification, the surface area, pore volume and average pore size of 3D-Graphene were decreased due to the filling of $\text{Mg}(\text{OH})_2$ particles in the pore channel. Meanwhile, this surface property of the composite 3D-Graphene/ $\text{Mg}(\text{OH})_2$ -1 showed notable increasing in that of its exceptional distribution. Further, after 20 hydration/dehydration cycles the primary stable porosity structure of 3D-Graphene/ $\text{Mg}(\text{OH})_2$ (3D-Graphene/ $\text{Mg}(\text{OH})_2$ -2) were practically still there.

3.2. The heat storage performance and heat transfer behavior of 3D-Graphene/ $\text{Mg}(\text{OH})_2$ composite nanomaterial

As shown in Fig. 7a, the heat storage density of pure magnesium hydroxide reached 765 kJ/kg , indicating that $\text{Mg}(\text{OH})_2$ was suitable for highly efficient thermal energy storage. However, the productivity of synthesized $\text{Mg}(\text{OH})_2$ was only about 26.7% after 20 min hydration of MgO during material synthesis process, which was obtained based on the weight loss (10.7%) of $\text{Mg}(\text{OH})_2$ (Fig. 7b). And this result also indicated that the hydration rate of magnesium oxide was slow. The incomplete reaction led to low heat storage density (269 kJ/kg) Fig. 7.c showed the TG-DSC curve of 3D-Graphene/ $\text{Mg}(\text{OH})_2$. For this composed material after 20 min hydration, MgO was fully hydrated to $\text{Mg}(\text{OH})_2$, and the heat storage density of the composed materials reached 610 kJ/kg (Fig. 7c). In addition, wonderfully, the active component ($\text{Mg}(\text{OH})_2$) heat storage density value was larger, which equaled to overall composed material heat storage density (610 kJ/kg) of 3D-Graphene/ $\text{Mg}(\text{OH})_2$ -1 divided by $\text{Mg}(\text{OH})_2$ content (47%) in the composed material. And the value could reach 1298 kJ/kg .

Fig. 8a showed the heat storage performance cycling stability of $\text{Mg}(\text{OH})_2$. And the hydration/dehydration cycle process made use of the reversible chemical reaction: $\text{Mg}(\text{OH})_2 \rightleftharpoons \text{MgO} + \text{H}_2\text{O}$. Initially, the heat storage density of $\text{Mg}(\text{OH})_2$ was 269 kJ/kg , but the heat storage stability fell quickly after 5 hydration/dehydration cycles. When cycling reaction reached 20th, the heat storage density had decreased to 119 kJ/kg , only 44% of the initial value. As shown in Fig. 8b, the heat storage performance cycling stability of 3D-Graphene/ $\text{Mg}(\text{OH})_2$ was better than $\text{Mg}(\text{OH})_2$, especially, after 5 hydration/dehydration cycles. And even when the hydration/dehydration reaction proceeded to 20th cycle, the heat storage density (601 kJ/kg , Fig. 7c) of composed material 3D-Graphene/ $\text{Mg}(\text{OH})_2$ was almost not changed (601 kJ/kg , Fig. 7d, Fig. 8b). This test provided strong evidence for the good heat storage cycle stability of 3D-

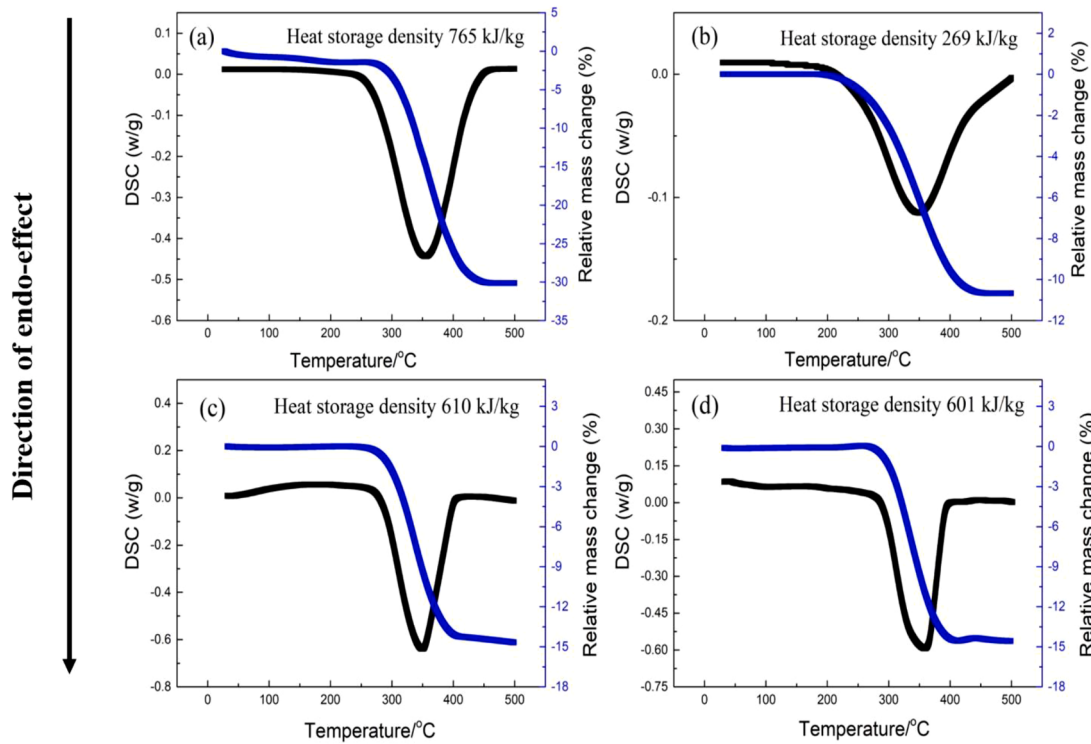


Fig. 7. TG-DSC curves of the samples: (a) pure $\text{Mg}(\text{OH})_2$, (b) $\text{Mg}(\text{OH})_2$ obtained after hydration of MgO , (c) 3D-Graphene/ $\text{Mg}(\text{OH})_2$ -1 before hydration/dehydration cycles and (d) 3D-Graphene/ $\text{Mg}(\text{OH})_2$ -2 after 20 cycles hydration/dehydration reaction.

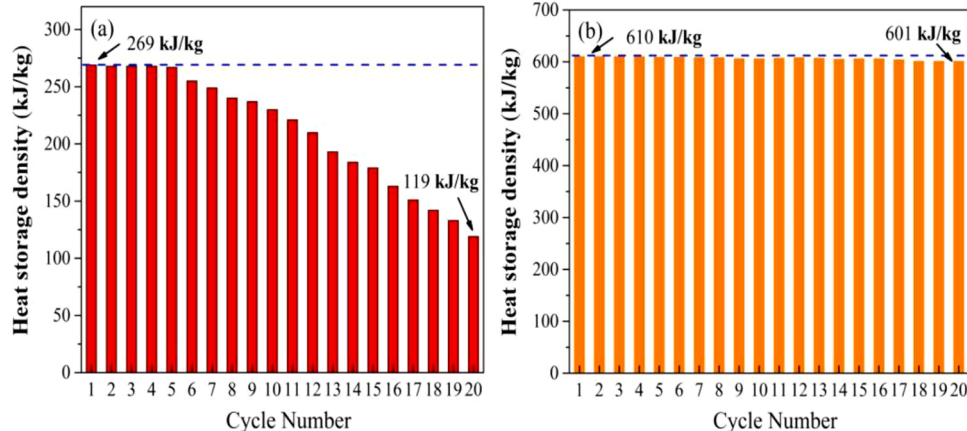


Fig. 8. Heat storage performance cycling stability of (a) $\text{Mg}(\text{OH})_2$ and (b) 3D-Graphene/ $\text{Mg}(\text{OH})_2$.

Graphene/ $\text{Mg}(\text{OH})_2$ composed material.

In order to explore the internal mechanism of heat storage performance enhancement, the kinetic behavior was investigated and the corresponding reactions activation energy were obtained. Fig. 9.a-9c showed the straight line of arrhenius's equation and the reaction activation energy calculated by ozawa method. As far as $\text{Mg}(\text{OH})_2$, the decomposition activation energy was extraordinarily high and reached 141.3 kJ/mol (Fig. 9a). But, when 3D-graphene composed with $\text{Mg}(\text{OH})_2$, the heat storage reaction became easier and the activation energy was decline to 116.7 kJ/mol (Fig. 9b). And after 20 hydration/dehydration cycles the activation energy (124.7 kJ/mol, Fig. 9c) was still lower than $\text{Mg}(\text{OH})_2$ (141.3 kJ/mol). It proved that addition of 3D-graphene could stably reduce the difficulty of the heat storage reaction.

According to the SEM (Fig. 3) and TEM (Fig. 4) results, the decreasing of decomposition reaction activation energy maybe relate to the micro shape of $\text{Mg}(\text{OH})_2$. When the majority of $\text{Mg}(\text{OH})_2$ particle

changed from bulk type (Fig. 3a) to nanoscale scaly type (Fig. 4b-4c) the heat storage reaction activation energy was 0.83 times lower. And when $\text{Mg}(\text{OH})_2$ particle changed to larger flower type (Fig. 3d) after 20 hydration/dehydration cycles the reaction activation energy slightly raised from 116.7 kJ/mol to 124.7 kJ/mol. It could be indicated from the micro structure and kinetic behavior of the 3D-Graphene/ $\text{Mg}(\text{OH})_2$ composed materials that the mechanism and process of heat storage reaction were different from single component $\text{Mg}(\text{OH})_2$ dehydration reaction. And the reaction activation energy, an important physical parameter for heat storage reaction, would change notably. Further, 3D-Graphene/ $\text{Mg}(\text{OH})_2$ provided enhanced reaction performance due to the nano-dispersion of $\text{Mg}(\text{OH})_2$, which enlarged the contact surface area of MgO and H_2O . And the unsaturated bonds in atoms of nanoparticles lead to better thermodynamic property [41,42]. Furthermore, the thermal conductivity of the 3D-Graphene/ $\text{Mg}(\text{OH})_2$ was 9.4 times higher than that of $\text{Mg}(\text{OH})_2$ (Fig. 9d). After that, in order to promote the matching

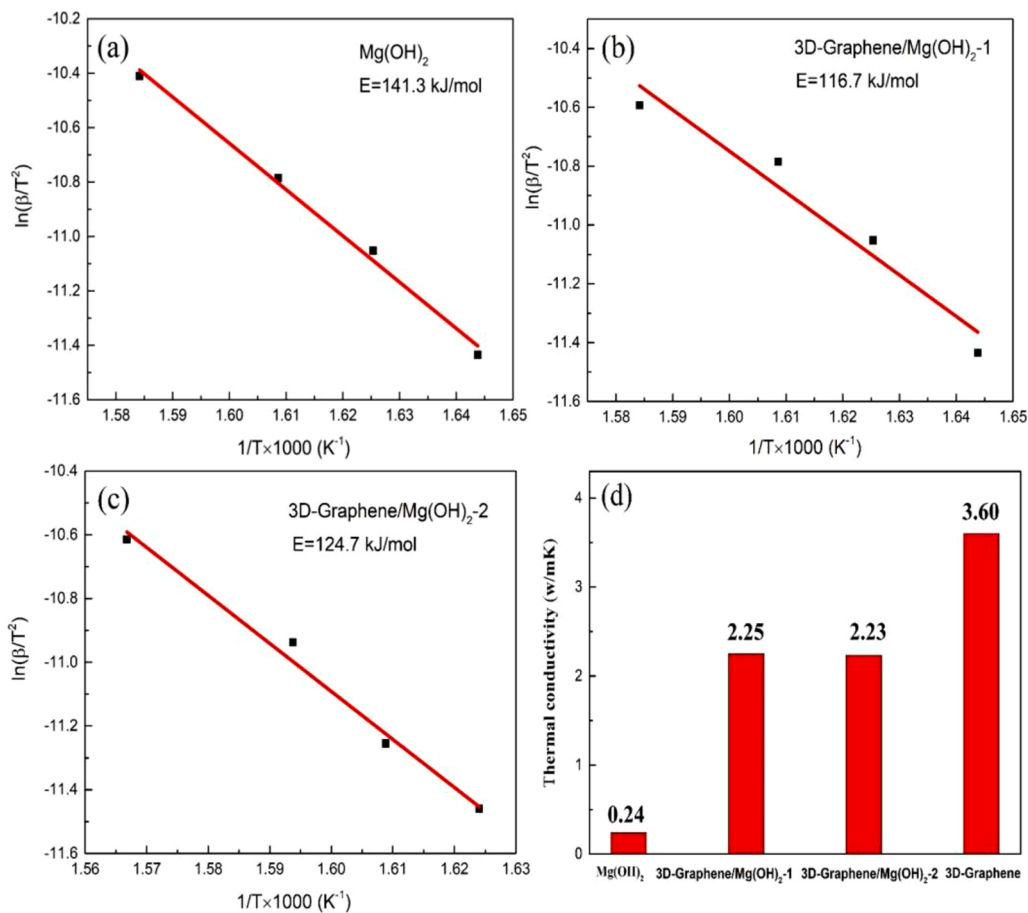


Fig. 9. The activation energy of dehydration reaction of (a) Mg(OH)_2 , (b) 3D-Graphene/ $\text{Mg(OH)}_2\text{-1}$ before hydration/dehydration cycles and (c) 3D-Graphene/ $\text{Mg(OH)}_2\text{-2}$ after 20 cycles hydration/dehydration reaction, (d) Thermal conductivity of Mg(OH)_2 , 3D-Graphene and 3D-Graphene/ Mg(OH)_2 .

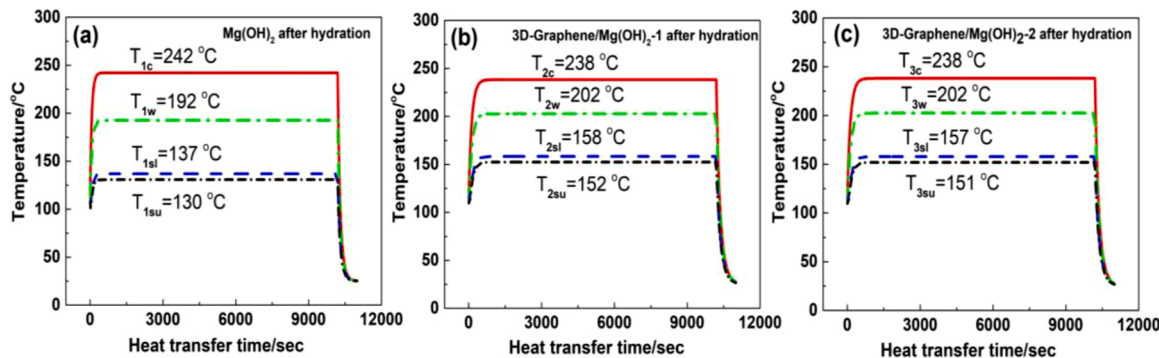


Fig. 10. Numerical simulation of temperature-time curves in reactor (a) Mg(OH)_2 , (b) 3D-Graphene/ $\text{Mg(OH)}_2\text{-1}$ before hydration/dehydration cycles and (c) 3D-Graphene/ $\text{Mg(OH)}_2\text{-2}$ after 20 cycles hydration/dehydration reaction.

degree and future application of these materials, the heat transfer behaviors of 3D-Graphene/ Mg(OH)_2 in stainless-steel reactor were simulated.

Fig. 10a-c were the numerical simulation temperature curves of the interface at different positions in the reactor when the heat storage materials Mg(OH)_2 , 3D-Graphene/ $\text{Mg(OH)}_2\text{-1}$ and 3D-Graphene/ $\text{Mg(OH)}_2\text{-2}$ were respectively filled in the reactor. All the temperature-time curves presented a trend of rapid rise of initial temperature, stable intermediate temperature and rapid drop of temperature. This was actually corresponding to the heat transfer process in the whole reactor, which was divided into three phases: exothermic heat of reaction was higher than heat elimination of environment leading to endothermic

and quick temperature rise of the whole reactor; the heat balance stage, when exothermic heat of reaction was equal to heat dissipation of the environment and no temperature change; the cooling stage of the reactor.

As shown in Fig. 10a the core temperature T_{1c} of Mg(OH)_2 in reactor was the highest, which was due to its lower thermal conductivity. Under the same heat dissipation conditions it lead to larger thermal resistance in the direction of reaction heat transferred along the perpendicular from the reactor center to the inner wall. The side inner wall temperature T_{1w} of Mg(OH)_2 in the reactor was 192°C . Material core temperature T_{1c} was 242°C . The difference in temperature reached 50°C (Fig. 10a). By comparison, the temperature gradient from the reactor

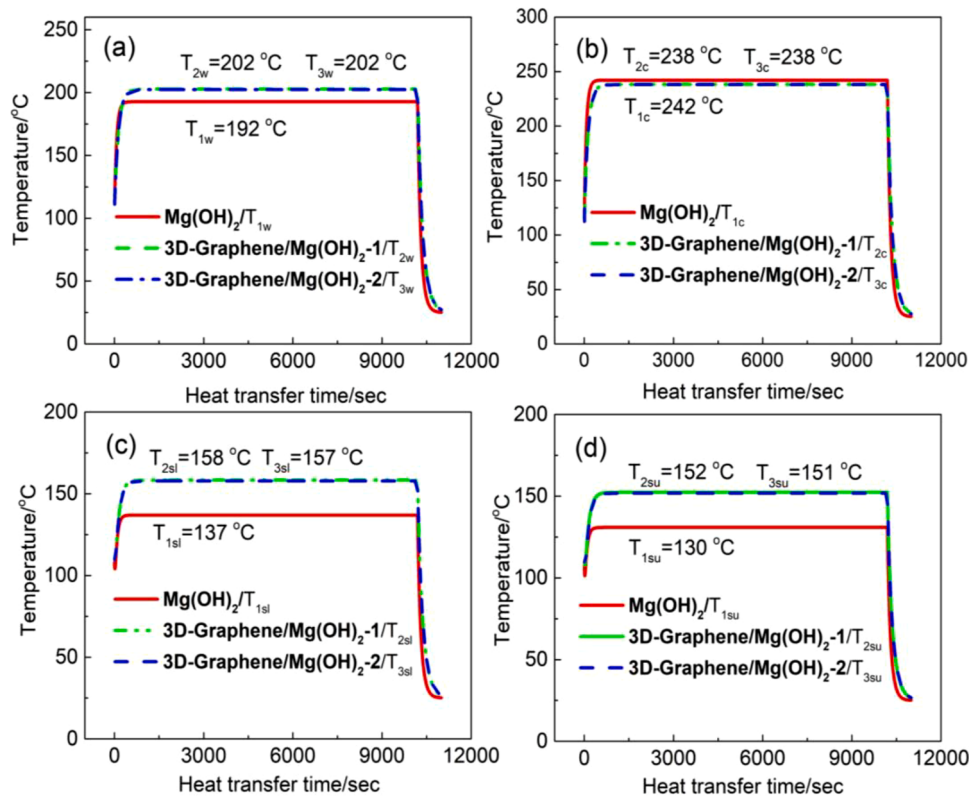


Fig. 11. Numerical simulation of (a) reactor wall temperature-time change comparison, (b) reactor core temperature-time change comparison, (c) heat storage material lower surface temperature-time change comparison and (d) heat storage material upper surface temperature-time change comparison of Mg(OH)₂, 3D-Graphene/Mg(OH)₂-1 before hydration/dehydration cycles and 3D-Graphene/Mg(OH)₂-2 after 20 cycles hydration/dehydration reaction.

center to the inner wall (Fig. 10a) was greater than that of composed heat storage materials 3D-Graphene/Mg(OH)₂-1 and 3D-Graphene/Mg(OH)₂-2 (Fig. 10b, Fig. 10c, difference in temperature: 36 °C). The characteristics of temperature distribution in the reactor was high temperature area in the center of reactor and low temperature area near the reactor wall. The average temperature T_{1sl} of the interface between N₂ gas with water vapor and Mg(OH)₂ at the lower surface (137 °C) was higher than the average temperature T_{1su} of the upper surface (130 °C) due to the bottom heat dissipation surface of the reactor was close to the ground, and its heat transfer capacity was less than that of the top (Fig. 10a). As a result, the heat dissipation capacity of the bottom layer material was not as good as that of the upper layer, and the released thermal energy mainly transferred through the side wall of the reactor.

Fig. 10b was the temperature time curve of the contact surface between heat storage material 3D-Graphene/Mg(OH)₂-1 and stainless-steel reactor. It can be seen that the temperature of material center

and contact interface between the heat storage material and the stainless-steel reactor could reach thermal equilibrium when the reaction lasted for about 500 s. The microstructure and heat transfer behavior of 3D-Graphene/Mg(OH)₂-2 that after 20 hydration/dehydration cycles (Fig. 10c) did not change significantly, and the heat transfer behavior was basically consistent with 3D-Graphene/Mg(OH)₂-1, which was tested before hydration/dehydration cycles.

Fig. 11a-d showed the temperature time curve comparison of the contact interface and reactor center among Mg(OH)₂; 3D-Graphene/Mg(OH)₂-1 and 3D-Graphene/Mg(OH)₂-2. The core temperature of Mg(OH)₂ was 242 °C. It was higher than that of 3D-Graphene/Mg(OH)₂-1 and 3D-Graphene/Mg(OH)₂-2 (238 °C). The reactor inner wall temperature reached 192 °C which was 10 °C lower than that of 3D-Graphene/Mg(OH)₂-1 and 3D-Graphene/Mg(OH)₂-2 (202 °C). Similarly, the average temperatures of the contact interface between N₂ gas mixed with water vapor and the sample at the upper and lower parts of the

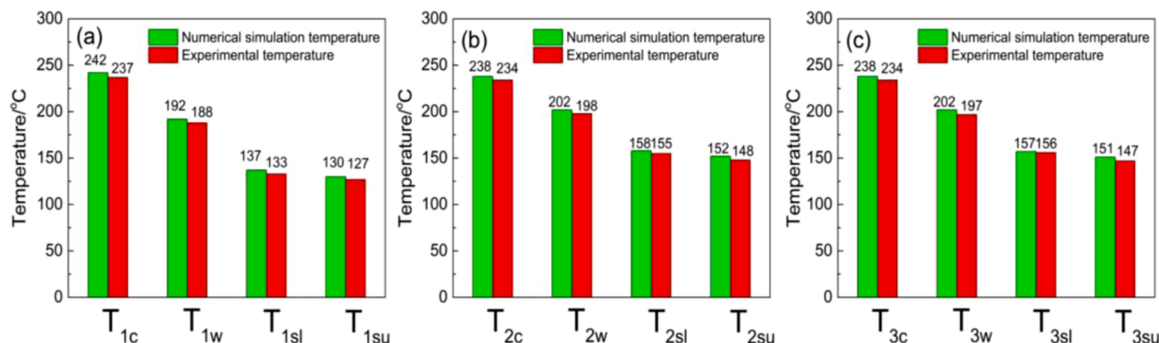


Fig. 12. The numerical simulation and experimental temperature data comparison for heat storage materials in the reactor (a) Mg(OH)₂, (b) 3D-Graphene/Mg(OH)₂-1 before hydration/dehydration cycles and (c) 3D-Graphene/Mg(OH)₂-2 after 20 cycles hydration/dehydration reaction.

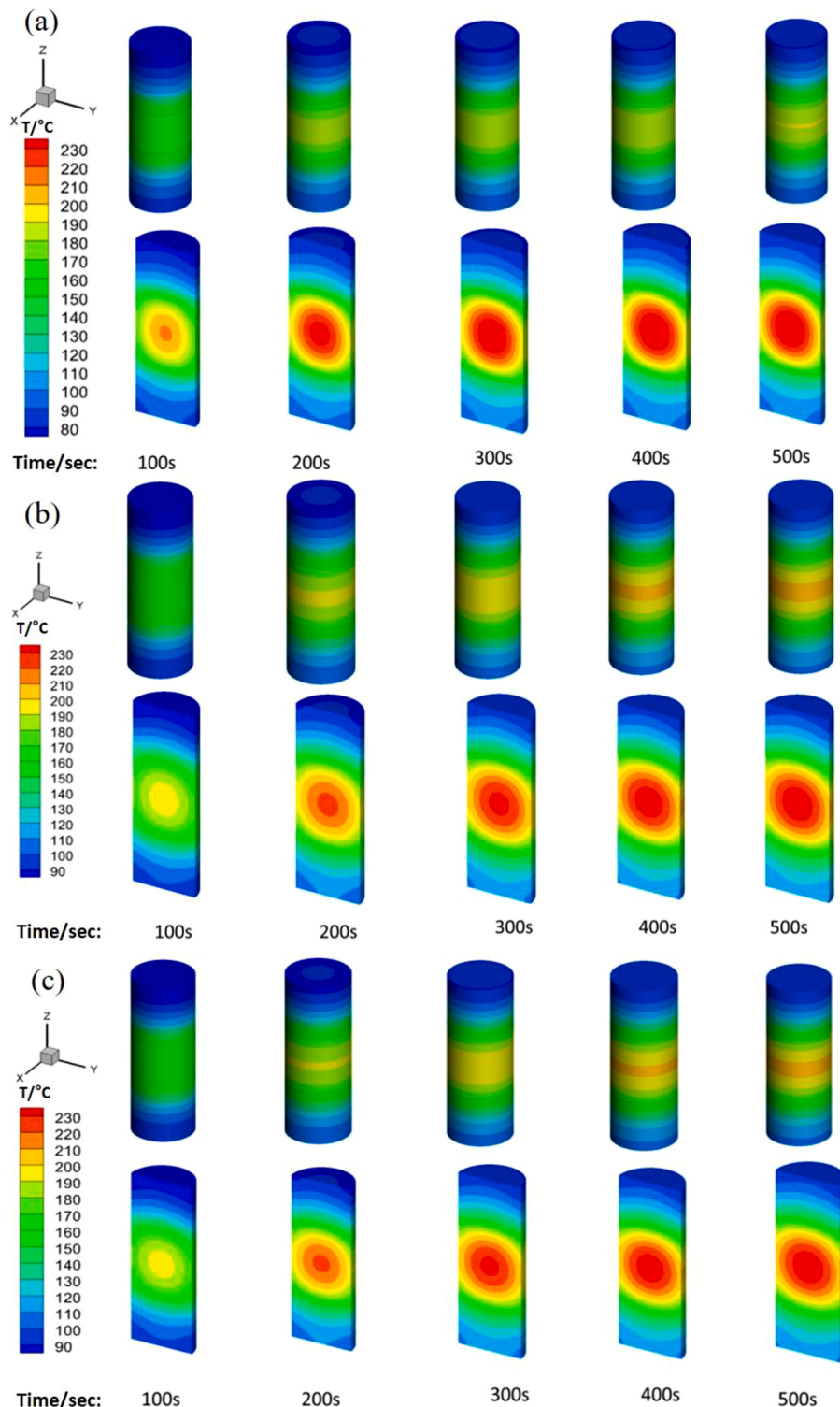


Fig. 13. The temperature distribution for heat storage materials in the reactor (a) $\text{Mg}(\text{OH})_2$, (b) 3D-Graphene/ $\text{Mg}(\text{OH})_2$ -1 before hydration/dehydration cycles and (c) 3D-Graphene/ $\text{Mg}(\text{OH})_2$ -2 after 20 cycles hydration/dehydration reaction.

reactor were also lower (temperature difference was at around 20 °C).

Fig. 12 showed the numerical simulation and experimental temperature data comparison for heat storage materials in the reactor. It could be seen that the simulation and experimental temperature (T_c , T_w , T_{sl} and T_{su}) of the materials were almost equivalent, respectively. It demonstrated that the numerical simulation of the heat transfer process was accurate and extremely valuable for future material and reactor design. The numerical simulation results of heat transfer process showed

that the heat transfer performance of composed heat storage materials 3D-Graphene/ $\text{Mg}(\text{OH})_2$ -1 and 3D-Graphene/ $\text{Mg}(\text{OH})_2$ -2 were better than that of $\text{Mg}(\text{OH})_2$ in stainless-steel reactor. For composed heat storage materials (3D-Graphene/ $\text{Mg}(\text{OH})_2$) the temperature gradient was lower and the chemical reaction was more evenly distributed in the reactor, which is more conducive to hydration reaction.

The physical model used for chemical heat storage material was a hollow cylindrical stainless-steel reactor (Fig. 1a). The heat transfer

process was investigated on the basis of which, a numerical calculation mesh 3D model was established (Fig. 1b). And then solved the energy conservation equation based on the finite volume method to simulate the heat transfer process in the reactor Fig. 13. showed the temperature distribution for heat storage materials in the reactor (a) Mg(OH)₂; (b) 3D-Graphene/Mg(OH)₂-1 before hydration/dehydration cycles; (c) 3D-Graphene/Mg(OH)₂-2 after 20 hydration/dehydration cycles. As shown in Fig. 13a-c, when the reaction progressed to 100 s, the temperature in the center of the reactor gradually raised and could reach above 190 °C. Because of low thermal conductivity and heat concentration of Mg(OH)₂. The central heating rate of the sample was faster and the core temperature was higher than that of 3D-Graphene/Mg(OH)₂-1 and 3D-Graphene/Mg(OH)₂-2. Mg(OH)₂ had a wider distribution of high temperature areas. As the reaction proceeded, the heat gradually released in the reactor and started to transfer from the center of the heat storage material to the surrounding, which caused the rearrangement of the temperature and finally reached heat balance. It can be seen from the temperature distribution, the wall temperature of 3D-Graphene/Mg(OH)₂-1 and 3D-Graphene/Mg(OH)₂-2 were higher than that of Mg(OH)₂, which related to their high thermal conductivity. The whole temperature evolution showed the dynamic change of temperature in the heat release process of reactor, which provided a advanced strategy for thermal energy utilization, subsequent synthesis of heat storage materials and the optimal design of the reactor.

4. Conclusions

In summary, 3D-Graphene/Mg(OH)₂ nanocomposite material was constructed, characterized, and applied for chemical heat storage. Mg(OH)₂ mainly dispersed to nanoscale (20–50 nm). The material showed an obviously enhanced heat storage density (610 kJ/kg) and addition of 3D-graphene led to a notable increase of the thermal conductivity of the composite material, which was 9.4 times higher than that of Mg(OH)₂. No distinct attenuation and greatly improved hydration rate compared with magnesium oxide because of hydrogen bonding effect in composite materials. 3D-Graphene lead to obvious decomposition activation energy decreasing of Mg(OH)₂ that would improve its utilization in the heat storage process. This was probably due to its surface effect. 3D-Graphene/Mg(OH)₂-1 showed the lowest activation energy (116.7 kJ/mol). According to the heat transfer numerical simulation, addition of 3D-Graphene could greatly change the temperature distribution in the reactor, it was easier to export thermal energy to the outside thermal load side. This energy storage system could output thermal energy at around 200 °C and absorbed heat at the range of 300–400 °C. The proposed method provided a facile and valid technique for thermal energy utilization and the synthesis of nano-composed materials with enhanced chemical heat storage performance.

Author contributions

This research was conceived and designed with the participation of all the authors. **Shijie Li** and **Xiangyu Yang** contributed equally to this work. **Shijie Li**: Conceptualization, Formal analysis, Investigation, Writing-original draft; **Xiangyu Yang**: Resources; Data curation; Writing-review & editing; **Xinyu Li** and **Wenshan Qu**: Visualization; **Tao Zhou** and **Ti Dong**: Validation; **Lisheng Deng**: Supervision; **Jin Zhang** and **Jianguo Zhao**: Supervision and Funding acquisition. All authors have read and agreed to the published version of the manuscript.

Author statement

Manuscript title: A high energy density 3D nano-carbon based magnesium hydroxide reversible chemical reaction heat storage material synthesis and heat transfer performance investigation. I have made substantial contributions to the manuscript, or design of the work; or the

acquisition, analysis, or interpretation of data for the work; I have drafted the work or revised it critically for important intellectual content; I have approved the revised version to be upload; I agree to be accountable for all aspects of the work in ensuring that questions related to the accuracy or integrity of any part of the work are appropriately investigated and resolved. All persons who have made substantial contributions to the work reported in the manuscript, including those who provided editing and writing assistance but who are not authors, are named in the Acknowledgments section of the manuscript and have given their written permission to be named. If the manuscript does not include Acknowledgments, it is because the authors have not received substantial contributions from nonauthors. Author: Shijie Li, Xiangyu Yang, Xinyu Li, Wenshan Qu, Tao Zhou, Ti Dong, Lisheng Deng, Jin Zhang, Jianguo Zhao

Declaration of Competing Interest

The authors declare no conflict of interest.

Funding

This work was supported by Key-Area Research and Development Program of Guangdong Province (Grant No. 2020B0202010004); National Natural Science Foundation of China (Grant No. 52071192).

References

- [1] A. Gil, M. Medrano, I. Martorell, A. Lázaro, P. Dolado, B. Zalba, L.F. Cabeza, State of the art on high temperature thermal energy storage for power generation, part 1-concepts, materials and modellization, *Renew. Sust. Energy Rev.* 14 (2010) 31–55.
- [2] Q.Q. Tang, J. Sun, S.M. Yu, G.C. Wang, Improving thermal conductivity and decreasing supercooling of paraffin phase change materials by n-octadecylamine-functionalized multi-walled carbon nanotubes, *Rsc Adv.* 4 (2014) 36584–36590.
- [3] V.A. Salomoni, C.E. Majorana, G.M. Giannuzzi, A. Miliozzi, R.D. Maggio, F. Girardi, D. Mele, M. Lucentini, Thermal storage of sensible heat using concrete modules in solar power plants, *Sol. Energy* 103 (2014) 303–315.
- [4] L. Miró, M.E. Navarro, P. Suresh, A. Gil, A.I. Fernández, L.F. Cabeza, Experimental characterization of a solid industrial by-product as material for high temperature sensible thermal energy storage TES, *Appl. Energy* 113 (2014) 1261–1268.
- [5] H. Wang, Y. Zhang, E. Ci, X.Q. Li, J.Q. Li, An experimental study in full spectra of solar-driven magnesium nitrate hexahydrate/graphene composite phase change materials for solar thermal storage applications, *J. Energy Storage* 38 (2021) 102536–102544.
- [6] Y.N. Liu, N.N. Wang, Y.F. Ding, Preparation and properties of composite phase change material based on solar heat storage system, *J. Energy Storage* 40 (2021) 102805–102822.
- [7] M. Rothensteiner, A. Bonk, U.F. Vogt, H. Emeriche, J.A.V. Bokhoven, Structural changes in equimolar ceria-hafnia materials under solar thermochemical looping conditions, cation ordering, formation and stability of the pyrochlore structure, *RSC Adv.* 7 (2017) 3797–53809.
- [8] E. Mastronardo, X. Qian, J.M. Coronado, S.M. Haile, Impact of La doping on the thermochemical heat storage properties of CaMnO_{3.8}, *J. Energy Storage* 40 (2021) 102793–102803.
- [9] P. Pardo, A. Deydier, Z. Anxionnaz-Minvielle, S. Rougé, M. Cabassud, P. Cognet, A review on high temperature thermochemical heat energy storage, *Renew. Sust. Energy Rev.* 32 (2014) 591–610.
- [10] H. Ishitobi, K. Uruma, M. Takeuchi, J. Ryu, Y. Kato, Dehydration and hydration behavior of metal-salt-modified materials for chemical heat pumps, *Appl. Therm. Eng.* 50 (2013) 1639–1644.
- [11] H. Ogura, T. Yamamoto, H. Kage, Efficiencies of CaO/H₂O/Ca(OH)₂ chemical heat pump for heat storing and heating/cooling, *Energy* 28 (2003) 1479–1493.
- [12] D.A. Sheppard, M. Paskevicius, C.E. Buckley, Thermodynamics of hydrogen desorption from NaMgH₃ and its application as a solar heat storage medium, *Chem. Mater.* 23 (2011) 4298–4300.
- [13] K. Kyaw, T. Shibata, F. Watanabe, H. Matsuda, M. Hasatani, Applicability of zeolite for CO₂ storage in a CaO-CO₂ high temperature energy storage system, *Energy Convers. Manag.* 38 (1997) 1025–1033.
- [14] X.X. Yang, H.Y. Huang, Z.H. Wang, M. Kubota, Z.H. He, N. Kobayashi, Facile synthesis of graphene oxide-modified lithium hydroxide for low-temperature chemical heat storage, *Chem. Phys. Lett.* 644 (2016) 31–34.
- [15] G. Balasubramanian, M. Ghommeh, M.R. Hajj, W.P. Wong, J.A. Tomlin, I.K. Puri, Modeling of thermochemical energy storage by salt hydrates, *Int. J. Heat Mass Trans.* 53 (2010) 5700–5706.
- [16] L. Farcot, N.L. Pierres, B. Michel, J.F. Fourmigué, P. Papillon, Numerical investigations of a continuous thermochemical heat storage reactor, *J. Energy Storage* 20 (2018) 109–119.
- [17] A. Malley-Ernewein, S. Lorente, Constructual design of thermochemical energy storage, *Int. J. Heat Mass Trans.* 130 (2019) 1299–1306.

- [18] C. Lehmann, O. Kolditz, T. Nagel, Modelling sorption equilibria and kinetics in numerical simulations of dynamic sorption experiments in packed beds of salt/zeolite composites for thermochemical energy storage, *Int. J. Heat Mass Trans.* 128 (2019) 1102–1113.
- [19] M. Kubota, S. Matsumoto, H. Matsuda, Enhancement of hydration rate of LiOH by combining with mesoporous carbon for Low-temperature chemical heat storage, *Appl. Therm. Eng.* 150 (2019) 858–863.
- [20] S.J. Li, H.Y. Huang, X.X. Yang, Y. Bai, J. Li, N. Kobayashi, M. Kubota, Hydrophilic substance assisted low temperature LiOH-H₂O based composite thermochemical materials for thermal energy storage, *Appl. Therm. Eng.* 128 (2018) 706–711.
- [21] M. Zamengo, J. Ryu, Y. Kato, Composite block of magnesium hydroxide-expanded graphite for chemical heat storage and heat pump, *Appl. Therm. Eng.* 69 (2014) 29–38.
- [22] S.T. Kim, J. Ryu, Y. Kato, Reactivity enhancement of chemical materials used in packed bed reactor of chemical heat pump, *Prog. Nucl. Energy* 53 (2011) 1027–1033.
- [23] Z.P. Zeng, X.C. Gui, Z.Q. Lin, L.H. Zhang, J. Yi, A.Y. Cao, Y. Zhu, R. Xiang, T.Z. Wu, Z.K. Tang, Carbon nanotube sponge-array tandem composites with extended energy absorption range, *Adv Mater.* 25 (2013) 1185–1191.
- [24] K. Zhang, T.T. Li, L. Ling, H.F. Lu, L. Tang, C.W. Li, L.J. Wang, Y.G. Yao, Facile synthesis of high density carbon nanotube array by a deposition-growth-densification process, *Carbon N Y* 114 (2017) 435–440.
- [25] H. Li, L.F. Liu, F.L. Yang, Covalent assembly of 3D graphene/polypyrrole foams for oil spill cleanup, *J. Mater. Chem. A* 1 (2013) 3446–3453.
- [26] E. Mu~noz-Sandoval, A.J. Cortes-Lopez, B. Flores-Gomez, J.L. Fajardo-Díaz, R. Sanchez-Salas, F. Lopez-Urías, Carbon sponge-type nanostructures based on coaxial nitrogen-doped multiwalled carbon nanotubes grown by CVD using benzylamine as precursor, *Carbon N Y* 115 (2017) 409–421.
- [27] J.K. Chen, X.C. Gui, Z.Q. Lin, Z.K. Tang, M.M. Lee, A. Wokaun, T. Lippert, Pulsed ultra-violet laser interactions with ultra-low-density porous carbon nanotube sponges, *Carbon N Y* 93 (2015) 604–610.
- [28] X. Su, J. Wu, B.J. Hinds, Catalytic activity of ultrathin Pt films on aligned carbon nanotube arrays, *Carbon N Y* 49 (2011) 1145–1150.
- [29] X.H. Cao, Y.M. Shi, W.H. Shi, G. Lu, X. Huang, Q.Y. Yan, Q.C. Zhang, H. Zhang, Preparation of novel 3D graphene networks for supercapacitor applications, *Small* 7 (2011) 3163–3168.
- [30] Y. Shen, D. Sun, L. Yu, W. Zhang, Y.Y. Shang, H.R. Tang, J.F. Wu, A.Y. Cao, Y. H. Huang, A high-capacity lithium-air battery with Pd modified carbon nanotube sponge cathode working in regular air, *Carbon N Y* 62 (2013) 288–295.
- [31] Q. Cao, S.J. Han, G.S. Tulevski, Y. Zhu, D.D. Lu, W. Haensch, Arrays of single-walled carbon nanotubes with full surface coverage for high-performance electronics, *Nat. Nanotechnol.* 8 (2013) 180–186.
- [32] M. Asif, Y. Tan, L.J. Pan, M. Rashad, J.Y. Li, X. Fu, R.X. Cui, Synthesis of a highly efficient 3D graphene-CNT-MnO₂-PANI nanocomposite as a binder free electrode material for supercapacitors, *Phys. Chem. Chem. Phys.* 18 (2016) 26854–26864.
- [33] L.M. Zhang, X.L. Sui, L. Zhao, G.S. Huang, D.M. Gu, Z.B. Wang, Three-dimensional hybrid aerogels built from graphene and polypyrrole-derived nitrogen-doped carbon nanotubes as a high-efficiency Pt-based catalyst support, *Carbon N Y* 121 (2017) 518–526.
- [34] Q.C. Wang, Y.P. Lei, Z.Y. Chen, N. Wu, Y.B. Wang, B. Wang, Y.D. Wang, Fe/Fe₃C@C nanoparticles encapsulated in N-doped graphene-CNTs framework as an efficient bifunctional oxygen electrocatalyst for robust rechargeable Zn-Air batteries, *J. Mater. Chem. A* 6 (2018) 516–526.
- [35] Z.P. Liu, R.Q. Zou, Z.Q. Lin, X.C. Gui, R.J. Chen, J.H. Lin, Y.Y. Shang, A.Y. Cao, Tailoring carbon nanotube density for modulating electro-to-heat conversion in phase change composites, *Nano Lett.* 13 (2013) 4028–4035.
- [36] S.J. Li, H.Y. Huang, J. Li, N. Kobayashi, Y. Osaka, Z.H. He, H.R. Yuan, The effect of 3D carbon nanoadditives on lithium hydroxide monohydrate based composite materials for highly efficient low temperature thermochemical heat storage, *RSC Adv.* 8 (2018) 8199–8208.
- [37] M. Kubota, S. Matsumoto, H. Matsuda, H.Y. Huang, Z.H. He, X.X. Yang, Chemical heat storage with LiOH/LiOH-H₂O reaction for low-temperature heat below 373K, *Adv. Mater. Res.* 953–954 (2014) 757–760.
- [38] D.S. Yuan, J.X. Chen, J.H. Zeng, S.X. Tan, Preparation of monodisperse carbon nanospheres for electrochemical capacitors, *Electrochim. Commun.* 10 (2008) 1067–1070.
- [39] S.K. Mehta, S. Kumar, S. Chaudhary, K.K. Bhasin, Effect of cationic surfactant head groups on synthesis, growth and agglomeration behavior of ZnS Nanoparticles, *Nanosc. Res. Lett.* 4 (2009) 1197–1208.
- [40] G.Q. Zhang, Z. Li, H.Y. Zheng, T.J. Fu, Y.B. Ju, Y.C. Wang, Influence of the surface oxygenated groups of activated carbon on preparation of a nano Cu/AC catalyst and heterogeneous catalysis in the oxidative carbonylation of methanol, *Appl. Catal. B Environ.* 179 (2015) 95–105.
- [41] B.X. Wang, L.P. Zhou, X.F. Peng, Surface and size effects on the specific heat capacity of nanoparticles, *Int. J. Thermophys.* 27 (2005) 139–151.
- [42] L.J. Chen, R.Q. Zou, W. Xia, Z.P. Liu, Y.Y. Shang, J.L. Zhu, Y.X. Wang, J.H. Lin, D. G. Xia, A.Y. Cao, Electro- and photodriven phase change composites based on wax-infiltrated carbon nanotube sponges, *ACS Nano* 6 (2012) 10884–10892.